The 9th European Congress on Computational Methods in Applied Sciences and Engineering
ECCOMAS Congress 2024
3 – 7 June 2024, Lisboa, Portugal

UQ ANALYSIS AND ROBUST OPTIMIZATION OF A TRANSONIC AIRFOIL FOR OPEN ROTOR DESIGN

QUENTIN BENNEHARD[*], GRÉGORY DERGHAM[†], JACQUES PETER[‡] AND MARCO CARINI[*]

[*] DAAA, ONERA, Institut Polytechnique de Paris, 92190, Meudon, France,
e-mail: {quentin.bennehard marco.carini}@onera.fr

[†]Safran Tech, DST Department, 78114 Magny-Les-Hameaux, France,
e-mail: gregory.dergham@safrangroup.com

[‡] DAAA, ONERA, Institut Polytechnique de Paris, 92320, Châtillon, France
e-mail: jacques.peter@onera.fr

Key words: Uncertainty Quantification, Robust Optimization, Polynomial Chaos, Open Rotor

Summary. This paper presents a comparison among efficient techniques for uncertainty quantification and robust optimization. Two test cases based on a thin airfoil representative of an open-rotor airfoil are studied at transonic conditions. The focus is on the precise estimation of the statistics of the aerodynamic coefficients. Thanks to two CFD-based surrogate models, the two test cases have been studied extensively without engaging the large computational cost normally associated with direct CFD evaluations. To address the high-dimensionality of the uncertainty space, we investigate two different approaches within the framework of generalized polynomial chaos expansion and least-square approximation for stochastic surrogate modeling. The first approach utilizes compressed sensing techniques, specifically Least Angle Regression and Basis Pursuit Denoising methods and the second approach named 'gradient-enhanced' least-square approximation, takes advantage of the adjoint capabilities of modern CFD solvers for efficient gradient computation. A combination of the two, associating gradient information with compressed sensing is also benchmarked.

1 INTRODUCTION

In recent decades, the significant advancements in computing power have propelled Computational Fluid Dynamics (CFD) to the forefront of industrial design, particularly in the aeronautical sector. However, it has become increasingly evident that discrepancies exist between the idealized conditions of numerical simulations and the complexities of real-world applications. This realization has spurred a growing interest in exploring the sensitivities of optimal shapes to uncertain parameters and in developing robust design techniques.

Uncertainties can be broadly categorized into two types: epistemic and aleatory. Epistemic uncertainties arise from our limited understanding and modeling of complex physical phenomena. In this context, Uncertainty Quantification (UQ) plays a crucial role in enhancing

the reliability of our physical models. On the other hand, aleatory uncertainties pertain to the inherent variability in shape or flow conditions, which, although uncontrollable, must be considered in the design process. Deviations from the intended design can occur due to manufacturing tolerances, as well as temporary and permanent degradation of aerodynamic surfaces over their lifespan. These phenomena will be particularly pregnant on open rotor blades, these blades having a complex aerodynamic design and being exposed to free flow during their life span.

To ensure the robustness of aerodynamic shapes obtained through numerical optimization, it is imperative to integrate uncertainties into the design process. While adjoint approaches in shape optimization have provided the capability to handle high-dimensional design spaces, the challenge of managing a large number of uncertain inputs, often referred to as the "curse of dimensionality," remains a significant bottleneck for the widespread application of UQ techniques in industrial settings, especially when coupled with High-Fidelity (HiFi) CFD simulations.

In this paper, we address the challenges posed by uncertainties in the context of transonic airfoil design for open rotor applications. For UQ methods, the focus of this paper will be on efficient polynomial chaos techniques which can afford a reduced number of expensive CFD computations: compressed sensing (Least Angle Regression [3], Basis Pursuit Denoising [9]) and adjoint-gradient enhanced variants [7], [8] of the standard least-square approximation. The open-source toolboxes *OpenTURNS* [5] (http://openturns.github.io/) and *eQuadrature* [4] (https://equadratures.org/) are used to apply these techniques on our test cases. The chosen test case is a 2D airfoil studied in transonic conditions, representative of the airfoil which could be found on open rotor blades. In a first step, shape design parameters are considered uncertain and a benchmark of the different methods is made on their ability to efficiently estimate the statistics associated with the aerodynamic coefficients. In a second step, a robust optimization is carried, considering uncertainties affecting the shape parameters.

2 METHODOLOGY

2.1 Uncertainty quantification

Polynomial Chaos Expansion is a well established approach [1] to derive a surrogate model approximating a function of interest $f(\boldsymbol{x})$ in the form of multivariate polynomials $H_{\boldsymbol{j}}(\boldsymbol{x})$:

$$f(\boldsymbol{x}) = \sum_{\boldsymbol{j}}^{\infty} c_{\boldsymbol{j}} H_{\boldsymbol{j}}(\boldsymbol{x}), \tag{1}$$

where $\boldsymbol{x}$ is a d-dimensional vector of independent random variables, $\boldsymbol{j}$ the multi-index associated with univariate polynomials and $c_{\boldsymbol{j}}$ the polynomial coefficients. The PCE coefficients can be computed by various methods. In particular, when considering non-intrusive techniques, the different approaches can be essentially divided into two families: i) *Spectral projection methods*, where the coefficients are computed by the numerical approximation of the projection of $f(\boldsymbol{x})$ on the orthogonal polynomial basis using classical Gauss quadrature and their more efficient sparse versions [13]. ii) *Collocation methods*, where the PCE coefficients are computed by fitting Eq. (1) to a given number of collocation points

in the uncertain space, to best reproduce the exact function value, leading to a classical Least Square Approximation (LSA).

2.1.1 Gradient-enhanced techniques

When gradient information is available, it can be used to introduce additional equations for the considered collocations points while reducing their number in order to achieve full rank. Since the gradient at each collocation point provides d additional scalar information, the total number of samples can be ideally reduced by the same factor with respect to the standard LSA formulation. However, attention has to be paid to accuracy issues in computing the derivative information, as often occurs for adjoint solvers employed in CFD applications. In order to reduce the sensitivity from numerical noise affecting the gradient accuracy, a null-space method has been proposed in [2] showing how this approach can achieve improved accuracy, especially for standard deviation, on a turbomachinery test case. The same method as implemented in the *eQuadratures* toolbox is employed here to compute the solution of the Gradient-Enhanced LSA (LSA-GE) problem.

2.1.2 Compressed sensing techniques

When dealing with very limited amount of data (e.g. as a direct consequence of expensive function evaluations) resulting in an underdetermined system for Eq. (1), an alternative solution can be sought in a sparse form, i.e. by minimizing the number of non-zero coefficients. Indeed, although real PCE models are not truly sparse, they are expected to be *compressible,* i.e. to feature a rapid decay in the magnitude of the coefficients at increasing order of the expansion, with most of the variance being captured by a few terms. This provides the rationale behind the compressed sensing approach leading to the Basis Pursuit Denoising (BPDN) [9] as well as to LARS [3] methods where the regressors are added according to their correlation with the current residual and the PCE coefficients are then updated using a least angle strategy. It should be noted that LARS with the LASSO (Least Absolute Shrinkage and Selection Operator) modification can be interpreted as a l_1-optimization solver. Both techniques, BPDN and LARS will be considered in the present study. In particular, for LARS, the implementation available in the open-source library *OpenTURNS* [5] is employed.

Moreover if gradient information is available, one can still search for a sparse PCE, using the compressed sensing techniques described above. This will lead to the BPDN-Gradient Enhanced (BPDN-GE) and the LARS-Gradient Enhanced (LARS-GE) methods. Only the first one has been implemented and tested in this work.

2.2 Robust optimization

In this section, we present the methodology employed to solve a robust optimization problem. Our approach involves formulating the objective and constraints as a linear combination of the statistical moments of one or multiple quantities of interest (QoI). These QoIs are considered stochastic due to their dependence on uncertain variables affecting the problem. While the distribution of the design variables is known, we leverage the previously discussed UQ techniques to efficiently compute the statistical moments of the QoIs at each iteration of the optimization process (Figure 1). The problem treated is of the following form:

$$\begin{aligned} &\text{Min } \mu_{Ca} + k\sigma_{Ca}, \\ &\text{With } \mu_{Cb} \geq \mu_{Cb_{target}}, \end{aligned} \tag{2}$$

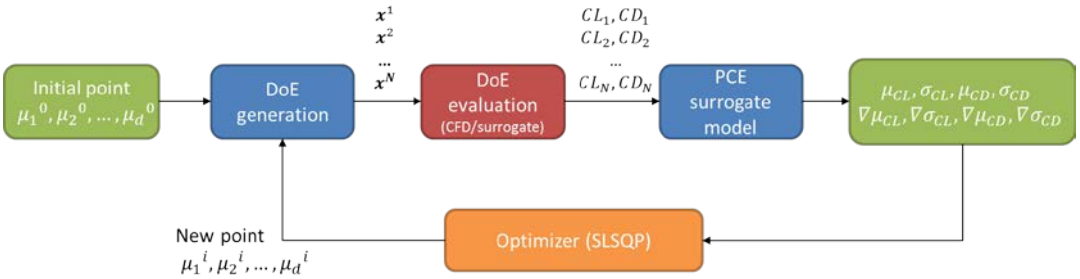

Figure 1: Robust optimization chain.

where μ and σ are the mean and standard deviation, respectively, Ca and Cb are generic aerodynamic coefficients, and k a multiplication factor. In this study, we restrict our attention to a problem where the design variables are all stochastics, we denote them as $\{x_i\}_{1\leq i\leq d}, d \in \mathbb{N}$. The variables considered by the optimizer are the mean of the design variables, noted $\{\mu_i\}_{1\leq i\leq d}$. Except for the variable mean, the PDF shape is considered constant across the design space, for all the design variables. This framework, although restrictive, still allows us to address relevant cases, such as when aerodynamic parameters are known with a certain level of precision or when manufacturing processes introduce constant variability in the shape. In this work, the robust optimization problem will be solved using gradient descent algorithms. A method to compute the gradient of the statistical moments is then needed. As explained in [7] §II.C.3, we leveraged PCE properties to compute theses gradients by finite difference, but without the need to perform additional DoEs.

3 TEST CASE

In this study we will use a test case defined in the frame of the NEXTAIR project by Safran. This test case is based on the study of a NACA 16-103 airfoil at transonic conditions. This airfoil has a maximum thickness of 3% and is chosen to be representative of an open rotor propeller at 75% span. It is simulated by solving the RANS equations, using the elsA code [6] (ONERA-SAFRAN property). The computations are performed on a structured mesh built around the airfoil using a O4H topology and featuring ~70k cells; the Roe's scheme is employed for the spatial discretization of the convective fluxes and the Spalart-Allmaras model for turbulence modelling. The considered reference flow conditions are Mach = 0.85, Altitude of 37000 ft and angle of attack of 1°. The International Standard Atmosphere (ISA) is used to obtain the density, dynamic viscosity and temperature at the chosen altitude leading to a Reynolds number of 3.66 million. The corresponding Mach field computed around the airfoil is illustrated in Figure 2.

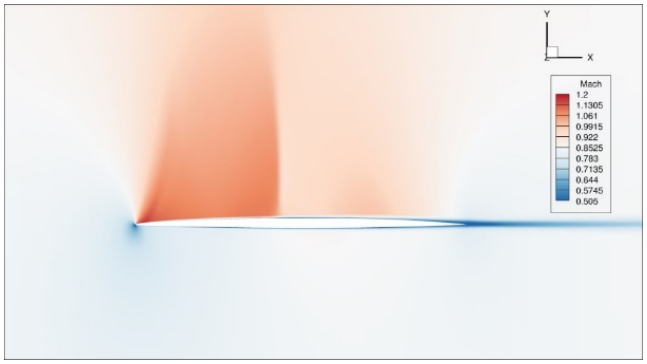

Figure 2: Mach field around the airfoil at the considered transonic conditions.

3.1 UNCERTAINTY QUANTIFICATION TASK

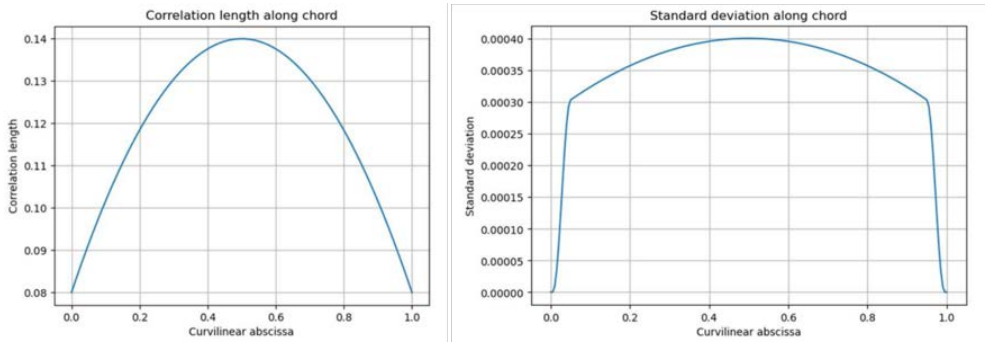

Figure 3: Correlation length (left) and standard deviation functions (right).

The fluid problem is made stochastic by introducing uncertainties, both on the shape of the airfoil and on the boundary conditions. To model the geometric uncertainties, a Gaussian deformation field is applied on each point of the airfoil, prescribing a normal displacement of the point. This Gaussian field, noted $g(m)$, is described by a covariance function given by Eq. (3) and a constant null mean. The variable m designs the curvilinear abscissa position, which

varies from 0 at the leading edge to 1 at the trailing edge.

$$cov(m_1, m_2) = \sigma(m_1)\sigma(m_2)\exp\left(-0.5\frac{(m_1-m_2)^2}{L(m1)L(m_2)}\right). \quad (3)$$

The correlation length function $L(m)$ is chosen such that it is smaller near the leading and trailing edge, and larger in the middle of the profile, following a parabolic function shown in Figure 3. The function $\sigma(m)$ is also chosen such that larger deformations are more likely to occur in the middle of the profile, but their amplitude decreases to reach 0 at the leading and trailing edge (Figure 3). Thanks to this covariance function and its mean, the Gaussian process is entirely defined and can be evaluated on every point of the mesh. However, for our application, we would like to model the shape uncertainty with a limited number of parameters. For that purpose, we perform a Karhunen-Loève (KL) decomposition of the Gaussian field, which can be written:

$$g(m) = \sum_{i=1}^{N_{modes}} \sqrt{\lambda_i}\phi_i(m)\xi_i. \quad (4)$$

where λ_i and ϕ_i are the eigenvalues and eigenvectors of the covariance matrix, respectively. ξ_i are mutually independent random Gaussian variables with zero mean and unit standard deviation. As the deformations along m are strongly correlated in space, the eigenvalue spectrum typically displays a very quick decrease, so one can truncate the KL expansion to a given number of modes. In this work, we decide to truncate the decomposition by using 5 modes since it guaranties to conserve the 94.47% of the total variance of the process. We impose independent deformation fields on the pressure and suctions sides of the profile and each of them is then described by 5 modes. As a result, the overall deformation field is parametrized by 10 variables, the 5+5 ξ_i normal variables. To insure numerical robustness, we decide to use truncated normal distribution between $[-3\sigma, 3\sigma]$ instead of the infinite support normal distribution for the ξ_i variables. Figure 4 presents nine realizations of the deformation fields. Once the $g(m)$ function is computed, it is used to deform the original mesh. Since the deformation magnitudes are small in this UQ task, the mesh quality metrics are kept very close from their original values. Figure 5 shows 100 deformed profiles resulting from the described parametrization.

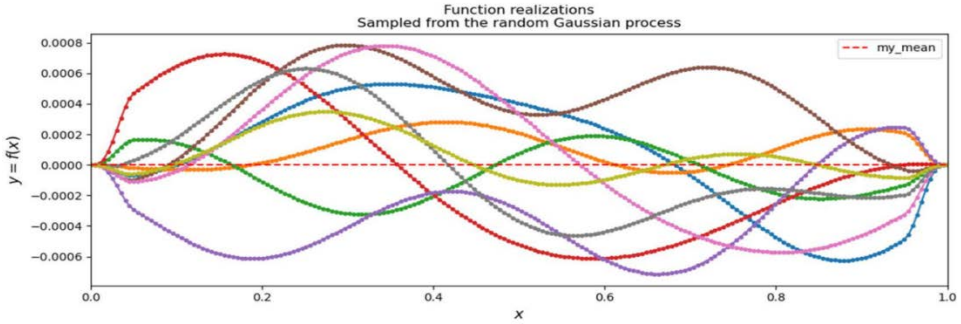

Figure 4: Realization of nine deformation fields

In addition to shape uncertainty, uncertainties affecting two aerodynamic conditions are also

considered: the free flow temperature and the infinite velocity. These variables are made uncertain by adding to them a term following a Beta distribution. To sum up, this test case has twelve uncertain variables:

- $\xi_i, i \in [1,10]$ follow a truncated normal Gaussian with $\mu = 0$, $\sigma = 1$, between $[-3,3]$.
- ΔT follows a Beta(4,4) distribution between bounds $[-2,2]\ K$.
- ΔV_{inf} follows a Beta(4,4) distribution between bounds $[-1,1]\ m/s$.

As a first step towards the use of this test case in a UQ context, a surrogate model was developed by Safran to reduce computational cost typically associated with CFD simulations. The construction of this surrogate model involved a two-step process. Initially, a Design of Experiment (DoE) comprising 300 simulations within the 12-dimensional design space was performed. Subsequently, a Kriging model was employed to enrich the DoE by sequentially adding samples in regions with the highest Drag variance, up to a total of 600 CFD runs. Three Kriging models are made on these 600 computations, to model respectively the lift, the drag and the glide ratio coefficients. These models are validated computing Q2 cross validation scores, which are all above 0.94 (the lowest value being obtained for the glide ratio).

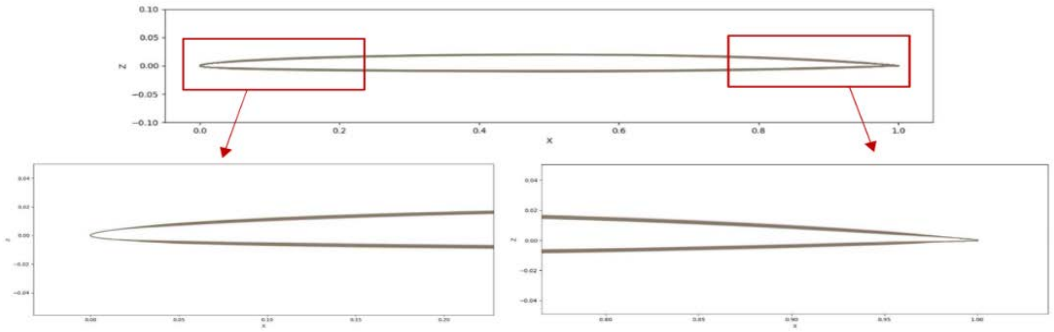

Figure 5: Sampling of 100 generated surfaces owing to the prescribed geometric uncertainty fields.

3.2 Robust optimization task

For the robust optimization task, a different parameterization was introduced consisting of 14 design variables which affect the shape of the propeller profile. Five design variables are used to control the camber law of the airfoil, on five control points equally distributed on the chord. In addition, five points are used to control the thickness distribution, keeping the maximum thickness constant. First the position of maximum thickness is made variable. Second, the thickness distribution is controlled by two control points at ¼ and ¾ of the chord, both on the pressure and suction sides (see Figure 6 bottom). Lastly, the leading edge and trailing edge radius can be modified by a multiplication factors, both on the pressure and suction sides, which adds four additional design variables. Similarly, to the UQ test case, a Kriging surrogate model was made at Safran, using a sequentially enriched DoE of 1200 CFD simulations.

This model can then be used to perform determinist optimization of the airfoil shape. To perform robust optimization, the 14 design variables are considered as stochastic variables.

After normalizing them between [0, 1], they are modeled by a Gaussian law with $\mu = 0.5, \sigma = 0.1$, truncated to lay between $[\mu - 3\sigma, \mu + 3\sigma]$. As explained in §2.2, the values of μ associated with the 14 PDFs of the uncertain design parameters are used as the unknown variables of the robust optimization problem. To avoid extrapolation outside the validity domain of the surrogate model, these variables are bounded between $\mu_i \in [0.3,0.7]$ so that they do not take values outside the $[0,1]$ range. The standard deviation is chosen to be quite large, to enhance high-order interactions in the stochastic problem.

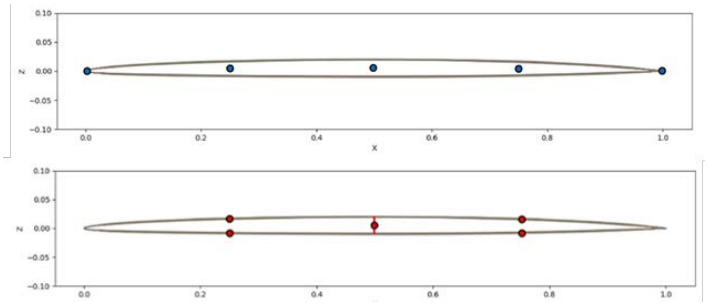

Figure 6: Position of the camber (top) and the thickness (bottom) control points.

4 UNCERTAINTY QUANTIFICATION RESULTS

4.1 Monte Carlo results

First, in order to provide reference values, statistical moments are computed by the Monte Carlo method on a large sample numbers of samples, of the order of ~10^8, obtained from the UQ surrogate model. The results are given with their 99% confidence interval. The following notation is adopted:

$$\mu_{Lift} = 4.123[86\ /93]\text{e-}01 \text{ means } \mu_{Lift} \in [0.412386, 0.412393], \tag{5}$$

Table 3: Reference values obtained by the Monte Carlo method.

Quantity	Lift	Drag	Glide Ratio
Mean	4.123[86/93] e-01	8.36[79/81] e-03	4.9281[40/94] e+01
Standard Deviation	1.214[37/82] e-02	2.264[00/84] e-04	1.032[42/79] e+00

4.2 PCE Results

In this section the results obtained with the different PCE methods mentioned in §2 are presented. They are presented as error color maps (Figure 7 and Figure 8), plotting the error with respect to the reference value obtained via the Monte Carlo analysis, as a function of the number of samples considered to build the PCE (y-axis), and of the order of the polynomial (x- axis). The error is expressed in percentage:

$$e(\gamma) = \left| \frac{\gamma_{ref} - \gamma}{\gamma_{ref}} \right| * 100. \tag{6}$$

The number of samples corresponds to the size of the DoE, which is here created by using a Sobol sequence. In this task, we look for a method that achieves the higher accuracy using the

smallest number of sample, as this number of sample is representative of CFD runs, when a high-fidelity function evaluations are directly engaged in the optimization process. In Figure 7 and Figure 8 a “continuous” representation of the results by means of graphic interpolation is adopted for an improved illustration although quantities along both axes are integer-values functions.

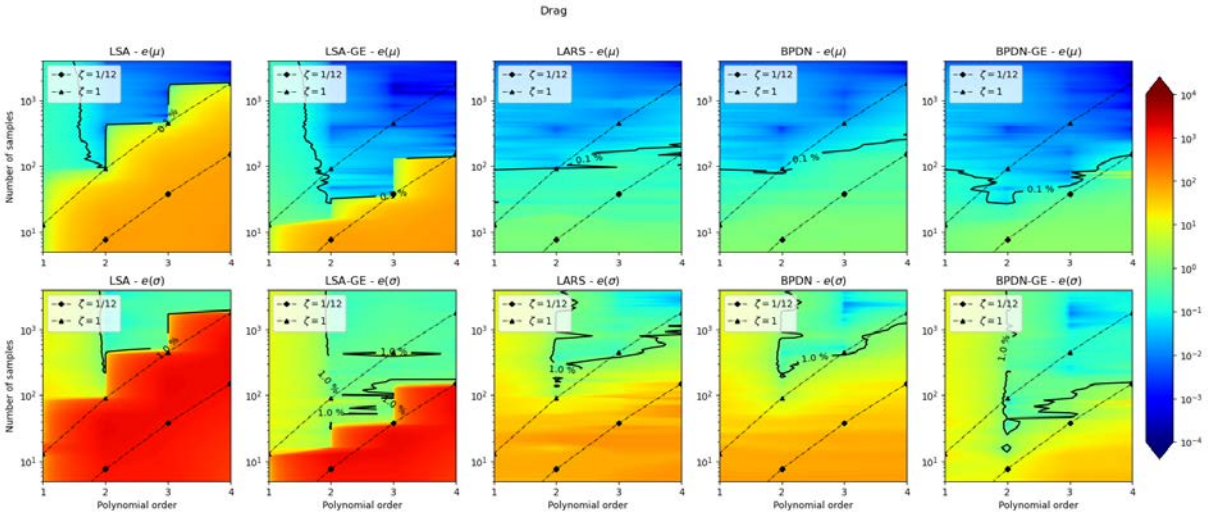

Figure 7: Error map for the mean (top) and the standard deviation (bottom) of the drag coefficient.

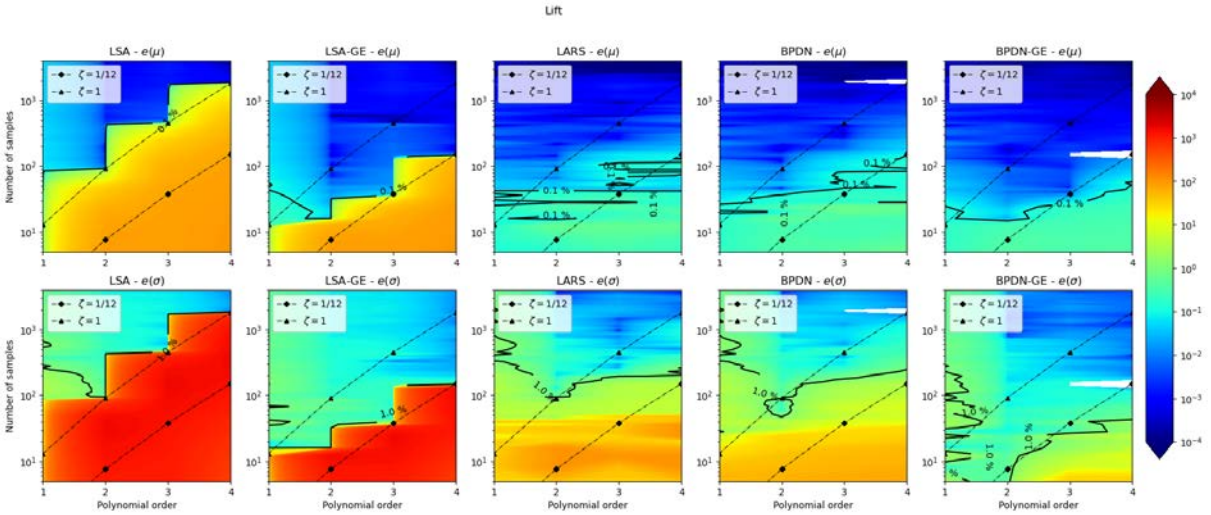

Figure 8: Error map for the mean (top) and the standard deviation (bottom) of the lift coefficient.

From these figures, we can see that the combination of compressed sensing and gradient information (BPDN-GE method) displays the best behavior. Thanks to this method, one can estimate with less than 1% error the standard deviation of the drag with a DoE of size 60, on an airfoil affected by 12 uncertain variables. If the gradient information is not available, the compressed sensing method LARS shows that one would need a DoE of size 140 to estimate the drag standard deviation with the same level of error, while the baseline method LSA

necessitates 230 samples to reach the same error level.

5 ROBUST OPTIMIZATION RESULTS

In this section, we present the results obtained on the robust optimization test case presented in §3.2, which has 14 design variables. The robust optimization problem considered is the following:

$$\text{Min } \mu_{CD} + 10\sigma_{CD}, \quad \text{With } \mu_{CL} \geq 0.4125. \tag{20}$$

To serve as a comparison point, a determinist optimization problem is also considered:

$$\text{Min } CD, \quad \text{With } CL \geq 0.4125. \tag{20}$$

As explained in §2.2, in the robust optimization, μ and σ are evaluated at each iteration of the optimizer by building a PCE with the relevant technique on a DoE of a certain size. The gradients of the statistical moments with respect to the design parameters (here the μ values parametrizing the PDF of the 14 design variables) are computed by finite differences, as previously mentioned. If the PCE method is not very efficient, a large DoE will be needed to estimate the moments of the aerodynamic coefficients, which will lead to a very large number of total calls to the CFD solver at the end of the robust optimization. Different PCE methods and DoE size have been tested on this test case, the results are presented in Table 4.

Table 4: Comparison of the results for the robust optimization test case using different UQ techniques. Reference deterministic optimization results are also included. Drag values are reported in drag counts (d.c.), i.e. as 1/10000 of the CD value.

	μ_{CD} (d.c.)	σ_{CD} (d.c.)	μ_{CL}	σ_{CL}	Optimizer iterations	DoE size	$f(\boldsymbol{x})$ Eval.	$\partial f/\partial x_j$ Eval.
Baseline	83.9	4.2	0.4124	0.022	-	-	-	-
Deterministic Optimization	**80.9**	2.5	0.4154	0.022	39	-	39	15
Robust Optimization LSA (Ref)	81.3	**1.8**	0.4142	0.020	30	480	14 400	-
Robust Optimization LSA	81.4	1.9	0.4160	0.020	21	240	5040	-
Robust Optimization LSA-GE	81.3	**1.8**	0.4142	0.020	54	30	1620	1620
Robust Optimization BPDN-GE	81.2	**1.8**	0.4143	0.020	23	30	690	690

Figure 9 presents the PDFs of the drag coefficient of the different shapes obtained by the different optimization processes. These PDFs have been obtained via a Monte Carlo analysis performed afterwards. One can observe that the deterministic optimization achieves a gain with respect to the baseline both on the mean of the drag (from 83.9 d.c. to 80.9 d.c.) and on its standard deviation (from 4.2 d.c. to 2.5 d.c.). All the robust optimization achieve similar

results, reducing further the drag variance (from 2.5 d.c. to 1.8 d.c.), at the cost of a slight degradation of the drag mean (from 80.9 d.c. to 81.2 d.c.). However, it is shown that the PCE methods that leverage the gradient information (LSA-GE and BPDN-GE) lead to an important reduction of the number of calls to the function evaluations that are necessary to perform the robust optimization. Here, we recall that CFD primal and adjoint runs are indeed replaced by the Kriging surrogate model. The BPDN-GE methods enabled the robust optimization with 690 equivalent primal and adjoint CFD runs leading to the same result obtained through more computationally expensive methods. Although this still represents a quite high computational cost, it is worth to remind that the treated problem has 14 dimensions, and that the cost of building the surrogate model was of 1200 CFD runs. In addition, further cost reduction can be expected when implementing a re-use strategy, which will allow one to re-use the points already computed in previous DoEs.

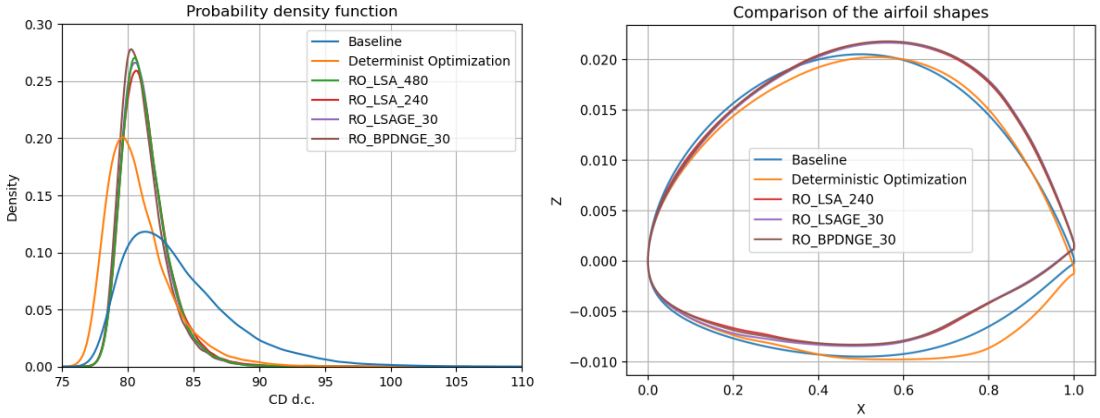

Figure 9: Probability density function of different airfoil shapes obtained by deterministic and robust optimization (left) and comparison of the resulting airfoil shapes (right).

6 CONCLUSIONS

This work treats an uncertainty quantification problem and a robust optimization problem with 12 and 14 uncertain parameters, respectively. Five methods to compute polynomial chaos expansion have been compared with the primary goal of minimizing computational costs (in the perspective of a CFD-driven process) while accurately estimating the mean and variance of the aerodynamic coefficients for a transonic airfoil representative of an open rotor blade. It is shown that 'gradient enhanced' and 'compressed sensing' methods can achieve significant performance gain when compared to the standard least-square approximation. More precisely, the method which combines the two approaches, BPDN-GE, achieves the most significant gain in both the uncertainty quantification and robust optimization tasks. On the UQ task the gain is a factor 4, while on the robust optimization, a factor 7 is found, compared to the classical least square approximation method.

On the robust optimization task, it has been shown that the efficient PCE methods allow a great reduction of the computational cost, which can become of the same order of the one associated to generation of the global surrogate or even smaller. Thus, such efficient UQ techniques can enable CFD-driven robust optimizations (to avoid surrogate modelling errors) and pave the way to treat more ambitious 3D cases. In addition, further cost reduction can be

expected by implementing a re-use of point strategy.

7 AKNOWLEDGMENT

This study is supported by the NEXTAIR project which has received funding from the European Union's Horizon Europe research and innovation program under grant agreement No 101056732. Views and opinions expressed are however those of the authors only and do not necessarily reflect those of the European Union. Neither the European Union nor the granting authority can be held responsible for them.

REFERENCES

[1] N. Lüthen, S. Marelli, B. Sudret, Sparse polynomial chaos expansions: Literature survey and benchmark. *SIAM/ASA Journal on Uncertainty Quantification* 9(2), 593-649, 2021.

[2] T. Ghisu, D. I. Lopez, P. Seshadri, S. Shahpar, Gradient-enhanced least-square polynomial chaos expansions for uncertainty quantification and robust optimization *in AIAA AVIATION 2021 FORUM (p. 3073).*

[3] G. Blatman, B. Sudret, Adaptive sparse polynomial chaos expansion based on least angle regression. *Journal of computational Physics*, 230(6), 2345-2367, 2011.

[4] P. Seshadri, G. Parks, Effective-Quadratures (EQ): Polynomials for Computational Engineering Studies. *The Journal of Open Source Software* 2(11), 166, 2017.

[5] M. Baudin, A. Dutfoy, B. Iooss, A.-L. Popelin, OpenTURNS: An Industrial Software for Uncertainty Quantification in Simulation, *Handbook of Uncertainty Quantification*, Springer International Publishing, 2001-2038, 2016.

[6] L. Cambier, S. Heib, S. Plot, The Onera elsA CFD Software: Input from Research and Feedback from Industry. *Mechanics and Industry*, 14(3), 159-174, 2013

[7] R. Mura, T. Ghisu, S. Shahpar, Least squares approximation-based polynomial chaos expansion for uncertainty quantification and robust optimization in aeronautics. *In AIAA AVIATION 2020 FORUM, p. 3163, 2020.*

[8] T. Ghisu, S. Shahpar, Affordable Uncertainty Quantification for Industrial Problems: Application to Aero-Engine Fans. *ASME. J. Turbomach*, 140(6): 061005, 2018.

[9] S. Chen, D. Donoho, Basis pursuit. *In Proceedings of 1994 28th Asilomar Conference on Signals, Systems and Computers*, 1, 41-44, 1994.